Cellular/Molecular

Action Potential-Evoked and Ryanodine-Sensitive Spontaneous Ca^{2+} Transients at the Presynaptic Terminal of a Developing CNS Inhibitory Synapse

Rossella Conti,[1] Yusuf P. Tan,[2] and Isabel Llano[1]

[1]Laboratoire de Physiologie Cérébrale, Université Paris 5, 75006 Paris, France, and [2]Bogazici Universitesi, Bebek, Istanbul 80815, Turkey

The existence of spontaneous calcium transients (SCaTs) dependent on intracellular store activation has been reported in putative axonal terminals of cerebellar basket interneurons. We used the two-photon imaging technique to optically identify basket terminals in acute cerebellar slices of young rats (11–16 d old) and study the properties of SCaTs unambiguously localized in these regions. The whole-cell recording configuration and preloading technique were alternatively used to load the calcium-dependent dye in the interneuron and compare SCaTs with action potential evoked calcium transients. SCaTs were observed in the basket terminals at frequencies that were significantly increased after bath application of 10 μM ryanodine and did not depend on P/Q- or N-type voltage-dependent calcium channel activation. They originated at specific sites where bursts of events with temporal separation as small as 200 msec could be generated. Their sites of origin were spaced on average 6 μm apart and were preferentially located near axonal endings. SCaTs had amplitudes comparable with those of Ca^{2+} rises evoked by single action potentials that lead to release of neurotransmitter, as confirmed by parallel recordings of preloaded terminals and evoked IPSCs in the postsynaptic Purkinje cells. These results support the hypothesis that SCaTs at basket terminals underlie the large miniature IPSCs characteristic of Purkinje cells.

Key words: **confocal imaging; presynaptic terminal; ryanodine; calcium stores; cerebellum; GABAergic**

Introduction

The basket–Purkinje cell inhibitory synapse of the cerebellar cortex is a very potent connection, with postsynaptic currents of the order of nanoamperes reported from dual patch recordings using postsynaptic symmetrical Cl^- concentrations (Vincent and Marty, 1996). Various lines of evidence indicate that ryanodine-sensitive Ca^{2+} stores contribute to GABA release at this synapse. It was shown that basket cell axons are rich in ryanodine receptors (RyRs), receptor-channel complexes located on the endoplasmic reticulum membrane that are responsible for Ca^{2+}-induced Ca^{2+} release (CICR) from intracellular stores (Pozzan et al., 1994; for review, see Berridge, 1998). The contribution of RyRs to spontaneous (Llano et al., 2000; Bardo et al., 2003) as well as evoked (Galante and Marty, 2003) GABA release has been documented. Furthermore, ryanodine-sensitive, spatially constrained Ca^{2+} elevations [called spontaneous calcium transients (SCaTs)] were demonstrated at hot spots of basket cell axons (Llano et al., 2000), which have been suggested to correspond to synaptic terminals (Forti et al., 2000). Spontaneous Ca^{2+} transients have also been observed at presynaptic boutons of hippocampal pyramidal cells (Emptage et al., 2001) and in frog vestibular hair cells (Lelli et al., 2003), in which electrophysiological studies support a role of RyRs on regulating transmitter release, and have recently been shown at nerve terminals from hypothalamic neurons (De Crescenzo et al., 2004). The observation of SCaTs adds to a growing body of evidence favoring the role of intracellular Ca^{2+} stores on exocytosis at various mammalian CNS synapses [CA3 hippocampal pyramidal cells (Savic and Sciancalepore, 1998); cortical pyramidal cells (Simkus and Stricker, 2002)], as well as in salamander photoreceptors (Krizaj et al., 2003) and at the neuromuscular junctions of frog (Narita et al., 1998) and lizard (Melamed-Book et al., 1993). Although the implication of Ca^{2+} stores in exocytosis is still controversial at some synapses (Carter et al., 2002; Lim et al., 2003), the available data indicate that the phenomenon may be widespread (for review, see Bouchard et al., 2003).

For basket–Purkinje cell synapses, a large fraction of synaptic contacts are formed right on the Purkinje cell soma, where many active zones are juxtaposed (Palay and Chan-Palay, 1974). Perisomatic synapses are likely to account for the large-amplitude miniature IPSCs (lamIPSCs) recorded from Purkinje cells (amplitudes of 200–1500 pA in symmetrical Cl^- conditions), which are selectively inhibited by high doses of ryanodine (Llano et al., 2000). The ryanodine sensitivity of both lamIPSCs and SCaTs suggests a causal relationship between the two types of events. To confirm this hypothesis it was necessary to demonstrate the presence of SCaTs at basket terminals and to investigate whether they

Received Dec. 20, 2003; revised June 18, 2004; accepted June 18, 2004.

This work was supported by European Community Grant QLG3-CT2001-02430, by the Centre National de la Recherche Scientifique (Unité Mixte de Recherche 8118), by Région Ile de France (Sésame Programme), and by a postdoctoral fellowship to R.C. from the "Fondation pour la Recherché Medicale." We thank P. Ascher and A. Marty for helpful comments on this manuscript, J. Chavas for helpful discussions throughout the work and comments on this manuscript, and M. G. Lucas for helpful discussions on the calcium-buffering mechanisms.

Correspondence should be addressed to Dr. Rossella Conti, Laboratoire de Physiologie Cérébrale, Université Paris 5, 45 rue des Saints Pères, 75270 Paris Cedex 06, France. E-mail: rossella.conti@univ-paris5.fr.

DOI:10.1523/JNEUROSCI.1397-04.2004

 0270-6474/04/246946-12$15.00/0

could potentially trigger vesicular release. This was the primary objective of the present work, which concentrates on the study of SCaTs at optically identified basket terminals onto the Purkinje cell body. In addition, we compared these signals with those induced by action potentials (APs) that trigger vesicular release during evoked synaptic transmission. An extensive study in the classic whole-cell configuration was complemented by the use of a preloading technique to characterize SCaTs in conditions that preserve synaptic transmission between cell pairs.

Materials and Methods

Slice preparation and electrophysiology. Acute sagittal cerebellar slices were obtained from 11- to 16-d-old Sprague Dawley rats that were decapitated after cervical dislocation. The cerebellum was removed rapidly and cut in ice-cold bicarbonate-buffered saline (BBS) containing (in mM): 130 NaCl, 2.5 KCl, 1.3 NaH_2PO_4, 26 $NaHCO_3$, 1 $MgCl_2$, 2 $Ca\,Cl_2$, 10 glucose, equilibrated with a mixture of 95% O_2 and 5% CO_2. In the same BBS solution, the slices were transiently transferred to a chamber at room temperature for 1 min and then kept at 34°C for 50 min. After this period, all slices were kept at room temperature until used in the experimental setup.

Whole-cell patch-clamp recordings were obtained from visually identified basket interneurons and Purkinje cells in slices perfused at 1.5 ml/min with BBS and maintained at room temperature on the stage of an upright microscope (Zeiss, Oberkochen, Germany). An EPC-9 double amplifier (HEKA Elektronik, Lambrecht/Pfalz, Germany) was used for data acquisition and electrical control. Recording electrodes were pulled from borosilicate tubing. For interneuron recordings, the intracellular solution was composed of (in mM): 140 K gluconate, 5.4 KCl, 4.1 $MgCl_2$, 9 HEPES, 3.6 ATP-Na, 0.36 GTP-Na, pH adjusted with KOH to 7.3, Osm 300. The Ca^{2+}-sensitive dye fluo-4 (Molecular Probes Europe, Amsterdam, The Netherlands) was used at a concentration of 400 μM in whole-cell recording (wcr) experiments and 800 μM in preloading experiments. The electrode resistance in the bath was of 9–11 MΩ. Interneuron recordings were performed in the voltage-clamp mode, with the holding potential kept at −78 mV. Series resistance values ranged from 25 to 50 MΩ and were compensated for by 50–70%. APs were generated by short (3 msec) depolarization of the soma to −10 mV, a protocol inducing an unclamped AP, which propagates along the axon. Current traces were acquired at a sampling frequency of 5–10 kHz. For Purkinje cell recordings, the intracellular solution contained (in mM): 150 KCl, 4.6 $MgCl_2$, 10 HEPES, 10 EGTA, 0.1 $CaCl_2$, 4 ATP-Na, 0.4 GTP-Na, pH adjusted with KOH to 7.3, Osm 300. The electrode resistance in the bath was 3 MΩ. Uncompensated series resistance ranged from 5 to 10 MΩ. Capacitive current cancellation and series resistance compensation were performed as described in Llano et al. (1991). Cells were maintained under voltage clamp at a holding potential of −68 mV (holding potential values are given after correction for liquid junction potential). TTX (0.2 μM; Sigma, St. Louis, MO), NBQX (1.5 μM; Tocris, Bristol, UK), and ryanodine (10 μM; ryanodine mixture, Calbiochem, La Jolla, CA) (from stock solutions in nanopure H_2O at 0.2, 1, and 10 mM, respectively) were added to the bath as stated in Results. Stock solutions of ω-conotoxin MVIIC (Tocris) were prepared at a concentration of 500 μM in nanopure H_2O and 1 mg/ml cyclosporin C, immediately frozen with liquid nitrogen, and stored at −80°C until use.

Detection and analysis of IPSCs were performed off-line with routines written in the IGOR-Pro programming environment (WaveMetrics, Lake Oswego, OR).

Ca^{2+} imaging system. Axons of interneurons within 60 μm from the surface of the slice were imaged with a two-photon laser scanning system, based on the design of Tan et al. (1999), with some modifications. Briefly, two-photon excitation of the Ca^{2+} probe was achieved with the beam of a Ti-sapphire laser (MaiTai, Spectra Physics, Mountain View, CA) set at an excitation wavelength of 820 nm. Rectangular regions on the sample were repetitively scanned by the laser beam, which was deflected in the *x–y* direction by two galvanometers. The beam was focused on the specimen through a Zeiss 63× water-immersion objective (0.9 numerical aperture) mounted on an upright microscope (Axioscop FS, Zeiss). The maximum average power at the specimen plane was kept under 7 mW to avoid photo damage. The area of the scanned region could be changed, with bigger areas corresponding to longer recording times per frame. Recordings at 10, 52, and 100 msec per frame were used in this work (corresponding imaged areas: 6 × 9, 23 × 9, and 17 × 24 μm; pixel size: 0.25 × 0.25 μm). The emitted light was focused on the active surface of an avalanche photodiode in photon counting mode (SPCM-AQR-13, PerkinElmer Optoelectronics, Fremont, CA) and sampled with a dwell time of 10 μsec. The light coming from the specimen could alternatively be sent to a Peltier-cooled CCD camera (PCO SensiCam) used for simultaneous transmitted light imaging of the slice and epifluorescence imaging of the axon excited by monochromatic illumination at 488 nm (TILL Photonics, Gräfelfing, Germany). At the end of the experiment, a camera image of the recording region was acquired, with both transmitted and fluorescent light turned on, to verify the colocalization of the axonal terminal and the Purkinje soma.

Image analysis. Off-line image analysis was performed with homemade software written in the IGOR-Pro programming environment. Raw data were loaded, and each pixel was multiplied by a conversion factor dependent on the signal amplitude to account for nonlinearities of the detector. A Gaussian filter of 3 × 3 pixel kernel was applied to each image. The absolute minimum count on the first image of a series was then taken and subtracted from all images to eliminate signal offsets in the electronics. No further baseline subtraction was performed.

To analyze series of scans, the average image over all scans was calculated. A line was manually traced on the image following the profile of the axonal branch (see Fig. 1*A*). A pixel-by-pixel interpolation of the manual line position was made, and the fluorescence values for each pixel on the line were taken as the average over a 3 × 3 pixel region centered on the pixel. These values were calculated for each image in the series to generate a two-dimensional (2D) image having on the *x*-axis the frame time, on the *y*-axis the pixel number, and as pixel pseudocolor the fluorescence value, which is reported in Hertz calculated from the number of photons acquired in 10 μsec sampling intervals. A $\Delta F/F_0$ image was then generated with the same *x–y*-axis but with pixel pseudocolor value corresponding to the percentage change in fluorescence for each pixel with respect to control as follows: $\Delta F/F_0\,(t,y) = [F(t,y) - F_0(y)]/F_0(y)$, where F_0 is the average fluorescence in control and F is the fluorescence at the same pixel at time t. In whole-cell experiments, in which APs were evoked by intracellular stimulation, the control period was chosen to be the eight images before stimulus onset. For SCaTs in whole-cell and preloading experiments and for spontaneous AP firing in preloading, the control period was chosen as 8–20 images before the event detection time. In cases in which event onset was early in the series of scans and no sufficient control period was available, F_0 was taken as the average fluorescence from the last scans in the immediately preceding series.

SCaTs origin detection. All *F* images were visually inspected to detect possible events, and $\Delta F/F_0$ was calculated as explained above. The event origin (y_0) was taken as the point of symmetry of the event in the $\Delta F/F_0$ image, which also corresponded to the point of earliest rise. All putative events visually detected were then confirmed as such by the following criteria: $\mathrm{Avg}(t,y_0) > 3 * \mathrm{stdev}/\mathrm{sqrt}(3) + \mathrm{baseline}$ for at least two consecutive points where $\mathrm{Avg}(t,y_0)$ is the average $\Delta F/F_0(y_0)$ over three time points starting at time t, baseline is the average $\Delta F/F_0(y_0)$ over 10 time points from $t - 13\Delta t$ to $t - 3\Delta t$, and stdev is the SD of the baseline. In the case of multiple signals, the baseline and stdev were calculated over a shorter interval starting after the peak of the previous response.

Amplitude and decay analysis. To obtain the peak amplitude and decay time constants of AP-evoked fluorescence changes in whole-cell recording experiments, single or double exponential functions were fitted to the decay of $\Delta F/F_0$ (y_0) versus time plots. For the temporal axis we used the actual time at which the selected pixel on the image was scanned. The temporal origin of the exponential fit was fixed as the time at which the last AP was fired. The slow decay of the transients assured us that no significant decrease in the amplitude of the signal occurred between the time at which the first and the last AP were fired. The fit was considered bi-exponential if the following criteria applied: (1) amplitude coefficients (A1, A2) were such that $0.15 < A1/(A1 + A2) < 0.85$, and (2) the ratio of the time constants of decay ($\tau 1$, $\tau 2$) was >3. In

this case the weighted time constant, $(A1 * \tau 1 + A2 * \tau 2)/(A1 + A2)$, was used to describe the time course of decay (τ_{decay}), and the peak amplitude was calculated as the sum of the two amplitude coefficients. Otherwise, parameters from a single exponential fit were used to describe τ_{decay} and peak amplitude. The choice of the weighted average was determined by the fact that the presence of parvalbumin at these terminals could result in a bi-exponential decay of the Ca^{2+} transients, as shown in chromaffin cells (Lee et al., 2000), which we observed in some regions. Previously published work on the same axons (Tan and Llano, 1999) reported the time to half-maximal decay of AP-induced fluorescence transients. This parameter preferentially captures the initial fast component of the decay and hence is smaller than the values reported in this work. Moreover, the choice of the Ca^{2+}-sensitive dye and its concentration are different in this work, because we wanted to be able to characterize a putatively variable range of Ca^{2+} signals. For the analysis of SCaTs and Ca^{2+} transients attributable to spontaneous firing in preloaded cells, we were faced with the problem that the signals decayed significantly within a frame time. We thus chose to characterize all transients at the regions that showed the highest fluorescence increments, assuming that they reflected regions that we happened to record soon after the signal initiated. A single exponential fit was used, and the temporal origin was fixed at the time of maximal amplitude increment. This method gives a slight underestimate of the actual amplitude. For multiple transients, in which the successive events appeared before the signal returned to baseline, data points were often insufficient to fit the decaying phase of the signals, and we limited the analysis to the time of event appearance.

Interevent intervals (IEIs) for SCaTs were calculated as the difference between the peak times of successive events, starting from the first event after ryanodine application. The IEI histogram was binned with a bin width of 0.5 sec in preloading experiments and 1 sec in whole-cell recording, and the cumulative probability was calculated from those histograms.

Cross-correlations ($r(k)$) were computed with the wrap-around method, on a discrete finite interval, using the following formula:

$$r(k) = \sum_i ([f(i) - mf] \times [g(i+k) - mg])/ \left[sqrt\left(\sum_i [f(i) - mf]\text{^}2 \times sqrt\left(\sum_i [g(i) - mg]\text{^}2 \right) \right) \right],$$

where f and g are the two functions for which the cross-correlation is computed, mf and mg are their means over the interval considered, and k is the pixel number along the line.

For statistical analysis, data from different recording sites of a given cell either were first averaged and the results from n cells pooled together to yield mean ± SD, or each site was treated separately as specified in Results. Statistical comparisons were performed using Student's t test. For the analysis of the change of the frequency of SCaTs after ryanodine application, the logarithm of the ratio of frequencies between ryanodine and control was taken for each cell, and the Student's t test was performed on this distribution.

Diffusion analysis. The equation used to estimate the diffusion coefficients in single events reflected passive diffusion from a point source in one dimension plus passive extrusion as follows: $F(x,t) = a * 1/\text{sqrt}(D * t) * \exp(-x\text{^}2/(4 * D * t)) * \exp(-k * t)$. Solution of the differential equation is as follows: $DF/dt = D * d^2F/dx^2 - kF$, with the constraints of $F(x,0) = 0$ and $F(x,\text{inf}) = 0$ and with a δ input at $x = 0$ at time $t = 0$. Fits of this equation to fluorescence data were performed on a point away from the source, with a sufficiently high baseline fluorescence to ensure a good signal-to-noise ratio. Only SCaTs that originated far from a branch point were considered, to satisfy the condition of diffusion in one dimension.

Results

Identification of the "basket" at basket cell–Purkinje cell synapses

Whole-cell voltage-clamp recordings were obtained from basket cells. The Ca^{2+}-sensitive fluorescent dye fluo-4 was introduced into the cell through the recording pipette. Approximately 10 min after break-in, it was possible to visualize the filled axon using two-photon laser scanning microscopy. The main axonal branch running parallel to the Purkinje cell layer and its ramifications toward Purkinje cells somata were explored. To aid in the identification of the terminals, the slice was also illuminated by transmitted light with oblique illumination and imaged with a CCD camera to visualize the Purkinje cells somata in the same field of view as the basket cell axonal branches. Switching back and forth from one kind of imaging to the other allowed the detection of axonal projections wrapping around the Purkinje cell body and making putative basket synapses onto it. It was considered that a connection existed when the two-photon image of the axon colocalized with the periphery of the Purkinje somata (Fig. 1*A*). The colocalization was verified at the end of the experiment with the CCD camera images of both transmitted and fluorescence light; an additional off-line check could be made because of the peculiar autofluorescence of the Purkinje cell body in the two-photon image (Fig. 1*A*,*B*).

Action potential-evoked signals at basket terminals

Once a terminal was found, a train of four APs was elicited by short repetitive depolarization through the somatic pipette to verify the activity of the terminal and obtain a reference signal for comparison with SCaTs. The Ca^{2+}-dependent fluorescence response was measured by repetitively scanning regions of 23 × 9 or 17 × 24 μm containing the terminal. Off-line analysis of the images was done by tracing a line through the center of the axonal terminal (Fig. 1*A*). The fluorescence along the line for each image and the relative fluorescence increase were calculated and the result plotted as 2D pseudocolor plots of F (Fig. 1*C*) and $\Delta F/F_0$ (Fig. 1*D*) along the axon (y-axis) versus time (x-axis). The peak amplitudes and time constants of decay were obtained by analysis of the $\Delta F/F_0$ plots as a function of time in 3 × 3 pixel regions (~0.56 μm^2) where SCaT signals could be detected (Fig. 1*E*). As discussed below, these regions did not always correspond to sites of high basal fluorescence or maximal response to AP firing. The average decay time, τ_{decay}, and peak $\Delta F/F_0$ values in 17 regions from 8 cells were 4 ± 2 sec and 250 ± 180%, respectively. These parameters varied significantly from terminal to terminal (corresponding coefficients of variation, 0.5 and 0.7).

Ryanodine-sensitive SCaTs present at basket terminals

Immediately after acquisition of AP-evoked signals, the experimental protocol to search for SCaTs started. Continuous recording of the terminal region was obtained by repetitive scanning in a series of 100 consecutive images with an interval for data storage of <1 sec between time series. A control period of 2–5 min with standard BBS was acquired, after which TTX and 4 mM Ca^{2+} were added to the bath solution to block voltage-dependent depolarization while maintaining active intracellular Ca^{2+} stores. After 4–7 min of continuous recording, ryanodine was added to the bath solution at a concentration of 10 μM to study the dependence of SCaTs on Ca^{2+} release from intracellular stores (Llano et al., 2000). In eight of nine experiments, SCaTs could be observed in the terminals. An example of SCaTs recordings is shown in Figure 2. The planar projection of the three-dimensional reconstruction of the basket terminal is displayed in Figure 2*A*, in which boxes are drawn around all regions where SCaTs were observed. The 2D pseudocolor plots in Figure 2, *C* and *D*, present the analysis for three consecutive scan series taken 1–2 min after ryanodine application, in terms of the absolute and relative fluorescence along the two lines drawn in Figure 2*B*, which shows the

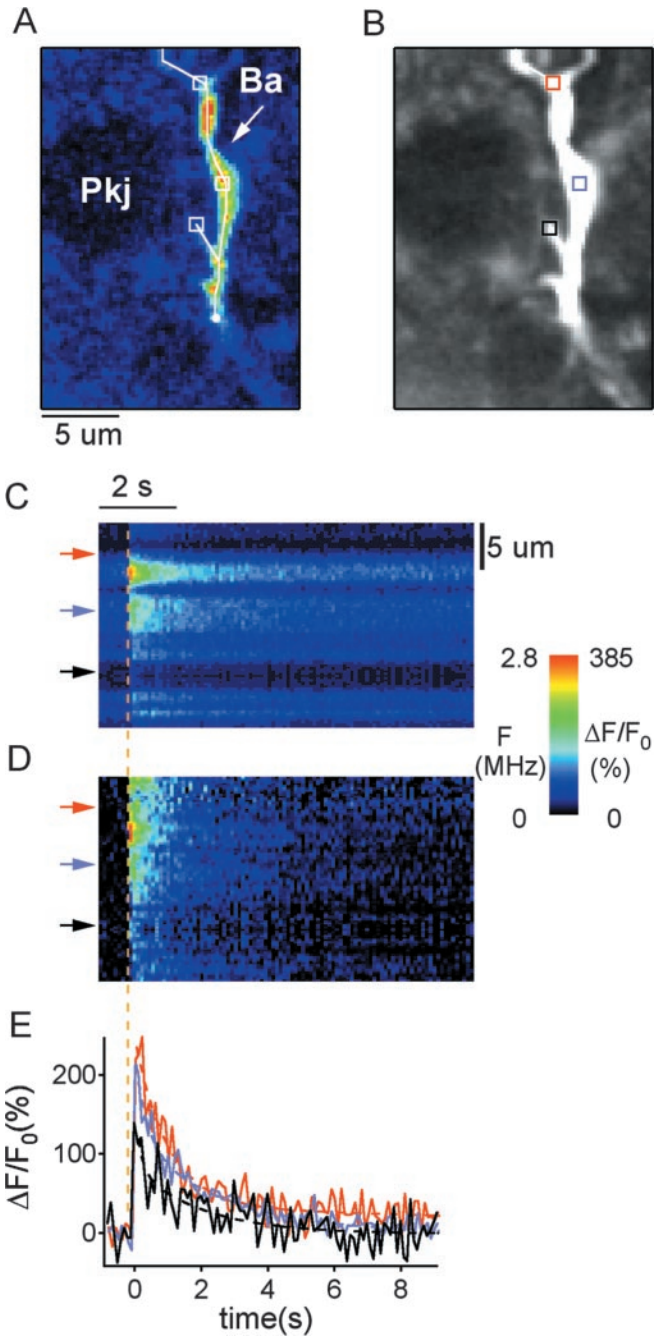

Figure 1. Action potential-evoked Ca^{2+} transients in basket cell terminals during whole-cell recording. *A*, Two-photon pseudocolor image of the fluo-4 fluorescence recorded from the axonal terminal formed by a basket cell (Ba) onto a Purkinje cell soma (Pkj). Images are averaged over eight consecutive scans acquired at rest with a dwell time of 100 msec per scan and covering a field of 17 × 34 μm (arbitrary units for the pseudocolor scale). *B*, Average of the same region, over 100 images, with grayscale chosen to enhance the autofluorescence of the Purkinje cell soma; axonal counts are saturated at this scale. *A*, *B*, Boxes indicate axonal regions that displayed SCaTs later in the experiment and the time course of which during AP firing is analyzed in *E*. *C*, *D*, Spatiotemporal profiles of the Ca^{2+}-dependent fluorescence (*C*) and the corresponding $\Delta F/F_0$ signals (*D*) along the line drawn in *A*. Time runs from left to right. The bottom left corner of the graphs corresponds to the end of the line marked by a filled circle in *A*. Colored arrows indicate axonal positions analyzed for time course in *E*, with color coding for each location. The dashed line marks the time when a 50 Hz train of four APs was delivered. *E*, Time course of the AP-evoked axonal $\Delta F/F_0$ signals measured at the locations indicated by arrows in *C* and *D*. The dashed traces present the fit of the decay phase by single exponential functions with the following amplitudes: 241, 216, and 152% and τ of 3.8, 1.6, and 1.2 sec.

image at the focal plane of recording. Two SCaTs can be clearly seen on the terminal region delimited by line 1 during the first scan series displayed, whereas the region along line 2 produced a single SCaT during the third scan series displayed. The temporal evolution at the site of origin for these SCaTs (Fig. 2*A*,*D*, arrows) is shown in Figure 2*E*, together with the diffused signals into a neighboring region.

In most cells, SCaTs were present in BBS as well as in 0.2 μM TTX, 6 mM Ca^{2+}_o, before ryanodine application. In all experiments, their frequency increased after application of ryanodine, with average frequency across cells of 0.01 ± 0.02 Hz in BBS, 0.008 ± 0.008 Hz in TTX, 6 mM Ca^{2+}_o (used as control), and 0.03 ± 0.03 Hz after addition of ryanodine (+ryan; $n = 8$ cells); see comparison in Fig. 3, *A* and *B*. The high variability in the frequencies reflects variability between cells. We thus calculated for each cell the ratio between event frequencies in control and after ryanodine application. In two cells in which no SCaTs were observed during the control period, the frequency was taken as 1/(observation time in control). The average ratio thus obtained was of 5 ± 6, indicating that ryanodine significantly increases the frequency of SCaTs observed at these terminals (*t* test on the distribution of the log of the ratios: $p < 0.005$; $n = 8$ cells). Ryanodine application did not cause a significant change in the amplitude of the signals ($\Delta F/F_0 = 400 \pm 400\%$ in control, $n = 6$ cells, vs $\Delta F/F_0 = 250 \pm 180\%$ after ryanodine application, $n = 8$ cells; $p > 0.2$).

Localization and temporal pattern of SCaTs

SCaTs recorded in ryanodine allowed the characterization of clear sites of origin from which diffusion into neighboring regions occurred. On each terminal we could identify between one and nine sites of origin, depending on the length that could be imaged at the same focal plane. The average number of sites was one every 6 μm (0.17 ± 0.07 sites per micrometer; $n = 8$ cells), with a preferential distribution near the endpoints of the terminal (in 9 of 10 axonal endpoints, a source of SCaTs was present within 1.5 μm; predicted from random distribution, 2.5 ± 1.1). The endpoints of terminals could be recognized by (1) no detectable basal fluorescence above autofluorescence values in the adjacent regions by visual inspection at different focal planes during the experiment and (2) the interruption of any fluorescence increase during a train of four APs.

During 8–15 min of recording, SCaTs occurred repetitively at the same sites. An interesting feature of these signals was that they often appeared in bursts. Thus, even if the average frequency over the total recording time was low, each site could generate a higher frequency of events during short intervals (Fig. 3*A*). To characterize this phenomenon, we calculated the IEI at each site, starting from the first observed event after ryanodine application and including all successive events observed (maximum recording time, 900 sec). The histogram for all sites that had more than two events was calculated and showed a peak at ~1–2 sec (Fig. 3*C*), with 50% of the events spaced by <5 sec, as shown from the cumulative probability plot for IEI in Figure 3*D*.

Amplitude and time course of SCaTs

Our measurements of the calcium-dependent fluorescence changes can give information about amplitudes and dynamics of the calcium signals within the optical resolution volume of the microscope. These values depend on the endogenous buffering and extrusion properties as well as on the nature of the added indicator dye (Neher and Augustine, 1992). No absolute values can be obtained with the non-ratiometric dye used, but it is still

possible to compare SCaTs with AP-evoked Ca^{2+} signals, provided that they are measured in the same buffering and extrusion conditions. Because of the diffusive nature of SCaTs, the decay time and amplitude of the relative fluorescence changes depend on the location where the signal is measured. We analyzed these parameters at the site of origin. SCaTs appeared either as single isolated events with a decay time that was fitted by an exponential function or as overlapping events too close in time to allow proper characterizing of the decay phase and amplitude. We therefore excluded these latter events from this analysis.

Figure 4 compares the properties of single SCaTs analyzed at each site of origin with the signal evoked by 4 APs at the same location (17 sites from 8 cells; like symbols indicate sites from the same terminal). There was no correlation between peak $\Delta F/F_0$ for the two types of signals (correlation coefficient: $\rho = -0.04$; $p > 0.5$; $n = 17$ sites) (Fig. 4*A*), whereas values for τ_{decay} were significantly correlated ($\rho = 0.68$; $p < 0.001$; $n = 17$ sites) (Fig. 4*B*). For these sites, ratios between transients elicited by four APs versus SCaTs were 4 ± 3 for peak $\Delta F/F_0$ and 2.4 ± 1.4 for τ_{decay}, respectively. This suggests that a single SCaT will have on average the amplitude expected from a single AP and faster decay time, if AP-evoked signals follow linear summation. Whether this linearity holds was verified in seven experiments by measuring the responses to one, two, and four APs. We found that peak $\Delta F/F_0$ values scaled linearly with the number of APs (amplitude ratios for four vs two APs: 2.1 ± 0.2; for two vs one AP: 1.9 ± 0.4; for four vs one AP: 3.9 ± 0.6; all not significantly different from the expected value if linear summation applies: $p > 0.2$, $p > 0.5$, $p > 0.5$, respectively; $n = 7$ cells). We then conclude that at their site of origin single SCaTs have on average the same amplitude as the signal evoked by one AP. In this same series of experiments, no difference was found for τ_{decay} between two and four AP-evoked transients (τ_{decay} ratios for four vs two APs: 1.02 ± 0.14; $p > 0.5$; $n = 7$ cells), whereas a significant difference was found between single and four AP-evoked signals (τ_{decay} ratios for four vs one AP: 1.4 ± 0.3; $p < 0.025$; $n = 7$ cells). Even taking into account the difference in τ_{decay} between one and four APs, SCaTs decay with a faster time course than that observed for AP-evoked signals ($p < 0.005$; $n = 17$ sites). A plausible interpretation of this difference lies in the nature of the two signals. SCaTs are highly localized in space, and their τ_{decay} will be determined most likely both by Ca^{2+} diffusion to neighboring regions with lower Ca^{2+}_i and by local buffering and extrusion. During an action potential, Ca^{2+}_i rises instead at multiple closely spaced sites, and there is thus little possibility for lateral diffusion. This leaves local buffering and extrusion as the main contributors to the decay of the signal. The diffusion constant for calcium in these experiments was calculated from two cells by fitting the diffusion of the SCaTs signal to a neighboring region (see Materials and Methods). This estimate was of 24 ± 18 μm^2/sec. Thus, in the case of AP signals, considering a spacing of 6 μm between the sources (Forti et al., 2000), the signal should equilibrate within ~360 msec.

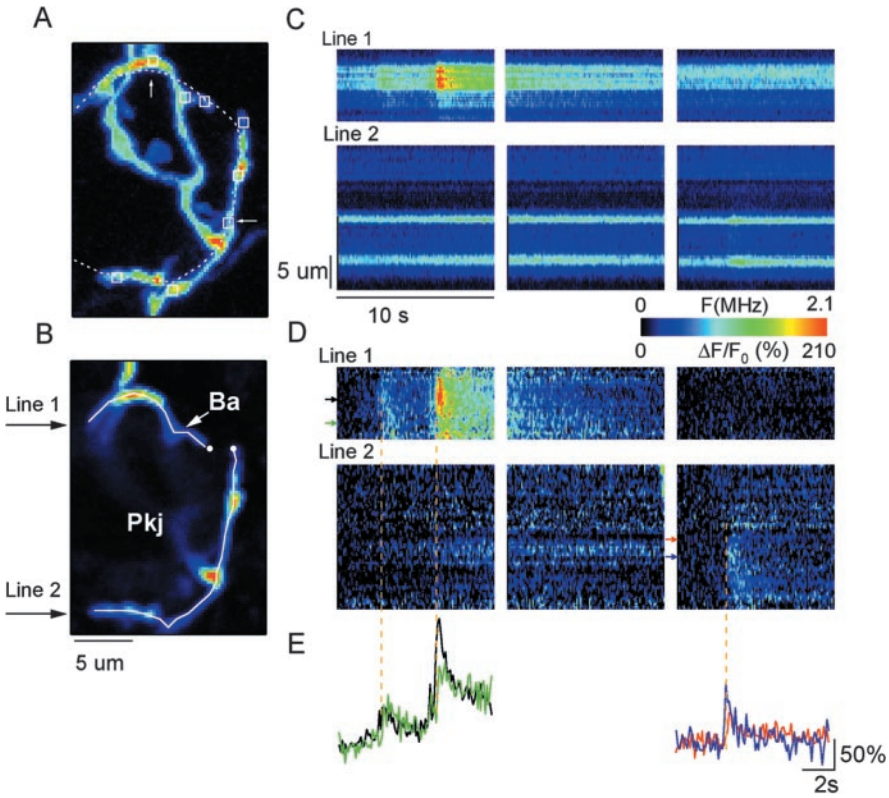

Figure 2. SCaTs in a basket terminal. *A*, Maximal intensity 2D projection of a three-dimensional reconstruction of a basket terminal from 20 scans obtained at rest at different focal planes (1 μm intervals). The 2D projection was made by taking the maximal fluorescence for each pixel over the 20 planes (arbitrary units). This reconstruction illustrates the extent of the basket terminal, which wraps around a Purkinje cell body (dotted line). Boxes delimit axonal regions that displayed SCaTs. Two of these regions (indicated by arrows) are analyzed in *C–E*. *B*, Average fluorescence image from 100 consecutive scans acquired at rest at the focal plane used for recording SCaTs. *C*, *D*, Spatiotemporal profiles of the [Ca^{2+}]-dependent fluorescence (*C*) and the corresponding $\Delta F/F_0$ signals (*D*) along the two lines drawn in *B*, recorded in the whole-cell recording configuration at −78 mV. The images correspond to a sample of consecutive time series acquired in the presence of 0.2 μM TTX, 6 mM Ca^{2+}, and 10 μM ryanodine. Note the multiple onset sites on this terminal. *E*, Time course of the $\Delta F/F_0$ transients measured at the locations indicated by the arrows in *D*; arrow color corresponds to the color used to plot each trace in *E*.

Amplitudes and kinetics for AP-evoked transients and SCaTs varied widely between experiments (Fig. 4*A*,*B*, like symbols). A likely explanation lies in the wide range of wcr times needed to find a terminal (from 14 up to 60 min). Two of the slowest τ_{decays} were measured in terminals found after >54 min from whole-cell break-in. In agreement with this interpretation, we found an inverse correlation between the τ_{decays} and the amplitudes of the AP-evoked signals, as shown in Figure 4*C* ($\rho = -0.5$; $p < 0.05$; $n = 17$ sites in 8 cells), which would support the idea of a difference in the buffering conditions among experiments. Additional contributions to the heterogeneity could arise from differences in the developmental stage of these terminals, which were not addressed in this work.

Furthermore, significant variabilities were found for sites in the same terminal, in agreement with previous reports of heterogeneities for AP-evoked Ca^{2+} signals in these axons (Forti et al., 2000) as well as in axons of pyramidal cells (Koester and Sakmann, 2000). The question arises as to whether sites for SCaTs generation are correlated with regions of maximal responses during AP firing. Analysis of the relative changes in fluorescence along the axon was performed for the two types of signals. As

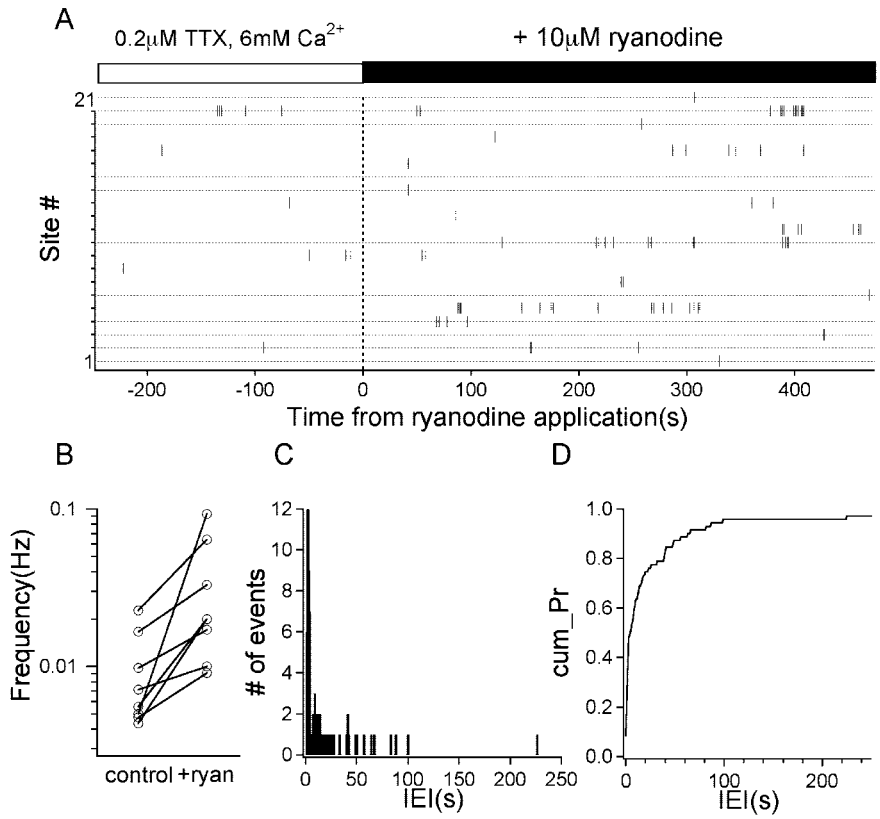

Figure 3. Ryanodine enhances the frequency of SCaTs at basket terminals. *A*, Plot of the time of appearance for each SCaT before and during ryanodine application (black bar on top of the graph) showing an enhancement in the number of SCaTs in the presence of ryanodine. Each level on the *y*-axis corresponds to a different site (21 sites from 8 cells). *B*, Average SCaT frequency in an external solution containing 0.2 μM TTX and 6 mM Ca^{2+} before (control) and after addition of 10 μM ryanodine (+ryan). Each pair of connected points corresponds to individual terminals, each from a different basket cell. *C*, Raw histograms of IEIs between successive SCaTs, analyzed for 14 sites in 7 axons that produced more than 1 SCaT. Bin width, 1 sec. *D*, Corresponding cumulative probability (cum_Pr) histogram.

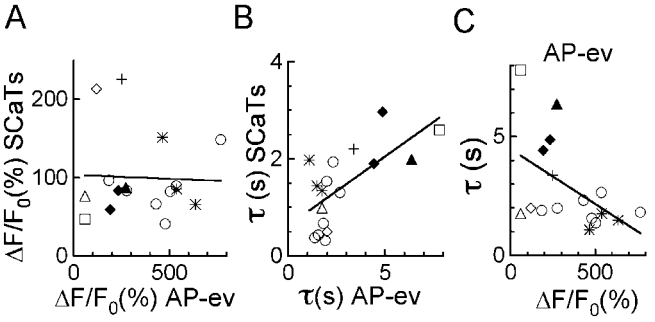

Figure 4. Comparison of SCaTs and AP-evoked Ca^{2+} transients in the whole-cell recording configuration. *A*, Peak values for $\Delta F/F_0$ transients of single SCaTs (*y*-axis) are plotted as a function of the peak value for the signal induced by a 50 Hz train of four APs (*x*-axis) at each axonal location that was a site of origin for SCaTs. Each symbol represents a different cell. The solid line corresponds to a linear regression fit of the data, with a slope $a = -0.01$ (correlation coefficient, $\rho = -0.04$; no correlation). *B*, Similar analysis for the time constant of decay (τ), which shows a significant correlation. Slope for the linear regression fit: $a = 0.33$ (correlation coefficient, $\rho = 0.68$). *C*, Plot of the time constant of decay as a function of the peak $\Delta F/F_0$ amplitude for the AP-evoked signals from the different recorded cells. The linear regression fit, with slope $a = -0.46$ sec/100% (correlation coefficient, $\rho = -0.5$), shows an inverse correlation between these two parameters (like symbols correspond to the same cell), indicating a possible difference in calcium buffering during different experiments.

exemplified in Figure 5*A*, SCaTs could sometimes be observed in regions that had a small response during AP firing. In this particular case, the typical bell-shaped spatial profile of a SCaT, measured in the first 100 msec from its appearance, is compared with the profile of the peak AP-evoked fluorescence response in the 100 msec after the last AP was fired. The SCaT originated on a region ~2 μm away from the local maximum of the AP-evoked signal. Similar profiles were generated for all sites of the three cells that had the longest axonal region in the focal plane (minimum, 11 μm). We then performed a cross-correlation analysis between the two traces to look for possible spatial correlations. The pooled data (Fig. 5*B*) showed no correlation of the AP-evoked signal on the distance from the SCaT origin, up to 6 μm away from it. In addition, for all cells that generated SCaTs, we determined the value of peak $\Delta F/F_0$ at the site of SCaT origin and compared it with the maximal value measured along the terminal. As shown by the histogram in Figure 5*C*, the peak amplitudes varied between 20 and 100% of the maximal peak $\Delta F/F_0$ (average: 65 ± 28%; $n = 17$ sites and 8 cells), supporting the notion that SCaTs are not correlated with sites of maximal calcium responses during AP firing.

Imaging the axons of preloaded interneurons

It has been reported previously that presynaptic whole-cell recording leads to an irreversible decline of evoked IPSCs at the basket–Purkinje cell synapse (Vincent and Marty, 1996; Pouzat and Hestrin, 1997; Diana and Marty, 2003). Total rundown of IPSCs occurs within 10–20 min of whole-cell recording (Diana and Marty, 2003), a time window shorter than that used for most of the whole-cell recording experiments presented above. Therefore, we sought to compare SCaTs and AP-evoked Ca^{2+} signals in experimental conditions in which synaptic transmission is maintained. For this purpose, we used a preloading technique in which interneurons were filled with the Ca^{2+}-sensitive probe in the whole-cell configuration for only 1–2 min, thus reducing washout of cytosolic components.

Basket cells were preloaded with fluo-4 by short whole-cell recordings on the soma. After <2 min after whole-cell break-in, we ascertained that the cell could generate APs and the pipette was withdrawn. If a high-resistance outside-out patch with voltage-gated K^+ currents remained in the pipette, the experiment was continued under the assumption that the basket cell soma had resealed correctly. After allowing 10–15 min for dye diffusion from the soma into the axon, we proceeded to search for a putative synaptic region as described for the whole-cell configuration. Because the basal fluorescence counts in this configuration were very low (average of 3 ± 1 photons per pixel in the brighter regions; $n = 8$ cells), extracellular stimulation was used to elicit AP firing and thus increase fluorescence to obtain a better visualization of the axon. Even during AP firing, it was sometimes

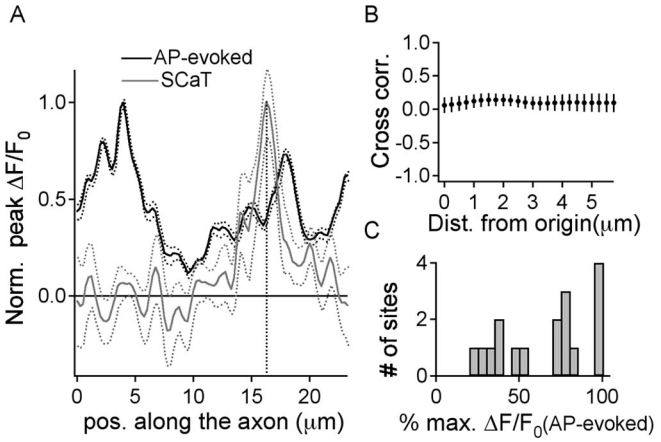

Figure 5. SCaTs origins do not colocalize with maxima of AP-evoked Ca^{2+} transients. *A*, Plot of the normalized peak $\Delta F/F_0$ responses versus position along an axonal terminal, 100 msec immediately after a train of four APs (black line) and in the first 100 msec from the appearance of a SCaT (gray line). Dotted lines represent $\Delta F/F_0 \pm 1$ SD. This example corresponds to the terminal region delimited by line 2 in Figure 2 *B*. The SCaT originates from a region of moderate response to AP firing, 1.75 μm away from a local maximum. *B*, Average cross-correlogram of the SCaT and AP-evoked transient profiles (12 representative SCaTs for each site of origin from 3 cells), centered at the SCaTs origin and pooled together as a function of the distance from the origin (both positive and negative directions are represented on the same axis). Error bars correspond to 1 SEM (15 traces). The cross-correlogram is not significantly different from 0 at any distance from the origins of SCaTs ($p < 0.05$; 2.5 SEM). *C*, The amplitude of the peak fluorescence response during AP firing at 17 sites of SCaT origin for 8 cells was compared with the maximal peak amplitude measured in the terminal, and the result is represented by the histogram of the normalized $\Delta F/F_0$ response.

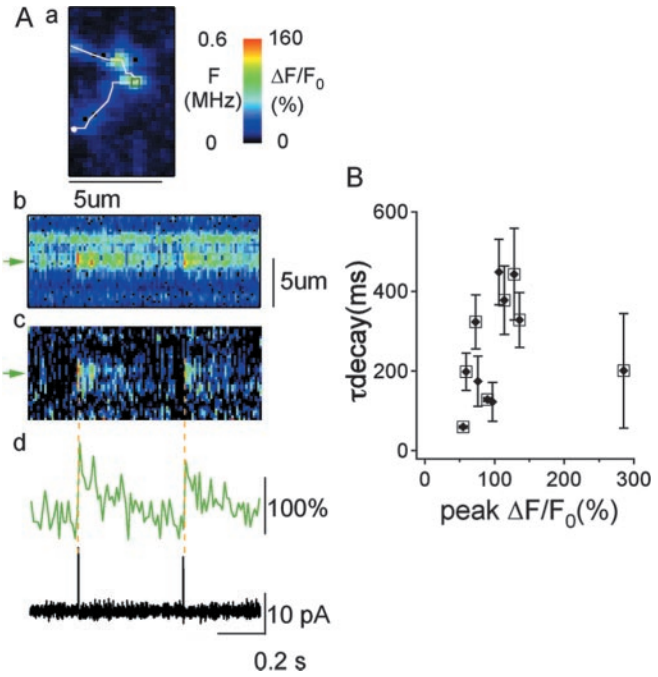

Figure 6. Spontaneous Ca^{2+} transients in axons of preloaded basket cells caused by spontaneous firing activity of the cell. *Aa*, Average fluorescence image (in arbitrary units) from 16 consecutive scans acquired at rest from a putative axonal varicosity of a basket cell preloaded with 800 μM fluo-4. *Ab*, *Ac*, Spatiotemporal profiles of the [Ca^{2+}]-dependent fluorescence (*Ab*) and the corresponding $\Delta F/F_0$ signals (*Ac*) along the line drawn in *Aa*. Arrows point to the location analyzed for time course in *Ad*, which is the only one showing Ca^{2+} transients. The color code calibration in *a* applies to *Ab* and *Ac*. *Ad*, Top traces, Time course of the $\Delta F/F_0$ signals in the location indicated by arrows in *Ab* and *Ac*. Bottom traces, Parallel cell-attached recording from the soma, showing the spontaneous firing activity of this cell. Note that the rising phases of the $\Delta F/F_0$ transients are correlated in time to an AP. *B*, Pooled data for the average peak amplitude (*x*-axis) and decay time (*y*-axis) from axons of 11 preloaded cells. Each symbol represents a different cell. Circles enclosed by open squares correspond to terminals on Purkinje cell soma.

hard to follow the axons because the AP-evoked fluorescence transients were restricted to small regions, whereas other regions (tens of micrometers long) did not have an appreciable fluorescence increase. As already mentioned, heterogeneity of AP-evoked fluorescence transients, albeit much less drastic, was also observed under whole-cell recordings.

Axonal fluorescence transients caused by spontaneous firing in preloaded cells

Because the cells were preloaded, they were not electrically perturbed and could fire spontaneously. In control conditions, in the absence of extracellular stimulation, continuous imaging of the axon revealed very rapid Ca^{2+} transients, which in some cases decayed to baseline within two time frames when recording at a rate of 100 msec per frame. This forced us to use faster scan rates and hence smaller areas (either 23×9 or 6×9 μm, 52 and 10 msec per frame, respectively). The signals were confirmed to be caused by spontaneous AP firing in one experiment in which a loose-patch recording was performed on the cell soma after preloading, allowing for the simultaneous recording of somatic APs and Ca^{2+} transients in a region of the axon in which AP signals could be detected (Fig. 6 *Aa*, box, *Ab*,*Ac*, arrows). As exemplified for the series of scans in Figure 6 *Ad*, all APs recorded from the soma fell within the rising phase of the axonal fluorescence transients, indicating that these transients are caused by spontaneous firing of the cell ($p \ll 0.0001$; $n = 35$ events).

In 11 basket cells, including the cell in Figure 6 *A*, Ca^{2+} transients similar to those described above were recorded. Eight of these experiments were conducted on putative terminals onto Purkinje somata, whereas the other three corresponded to recordings of axonal regions coursing the molecular layer, presumably containing en passant boutons. As shown in Figure 6 *B*, in which the former are enclosed in open squares, peak amplitudes and τ_{decay} did not depend on the type of region recorded. The signals, analyzed at regions that showed the highest fluorescence increment, were characterized by a fast rise time (within the frame rate, which was usually 10 msec), with peak $\Delta F/F_0$ of $111 \pm 64\%$ ($n = 11$ cells) and a decay that was fitted with a single exponential with a τ_{decay} of 0.26 ± 0.14 sec. This τ_{decay} was much faster ($p < 0.005$) than the one measured in whole-cell recording for single AP-evoked transients, even when compared with the signals in highly responsive regions and selecting only the cells that were kept in the whole-cell configuration for <35 min (τ_{decay} for one AP: 1.7 ± 1.5 sec; $n = 5$ cells).

Because the Ca^{2+} indicator acts as an exogenous Ca^{2+} buffer that adds to the endogenous buffering capacity, its intracellular concentration affects the time course of calcium transients. The large difference in τ_{decay} between whole-cell and preloading experiments can be expected in part by supposing a lower concentration of dye in the latter case. We made a rough estimate of the relative dye concentration in the two types of recordings by comparing the average resting fluorescence of the axonal regions recorded in wcr (F_{wcr}) and in preloading ($F_{preload}$). This evaluation is possible only because of the confocality of the excitation of the two-photon system. Differences in excitation and recording parameters were measured for each experimental day through a sample of 50 μM fluorescein and were corrected in the calculation. The ratio of Fwcr/Fpreload was 2.1 ± 0.7 ($p < 0.025$ of the fluorescence being equal; $n_1 = 8$ cells in wcr; $n_2 = 8$ cells in

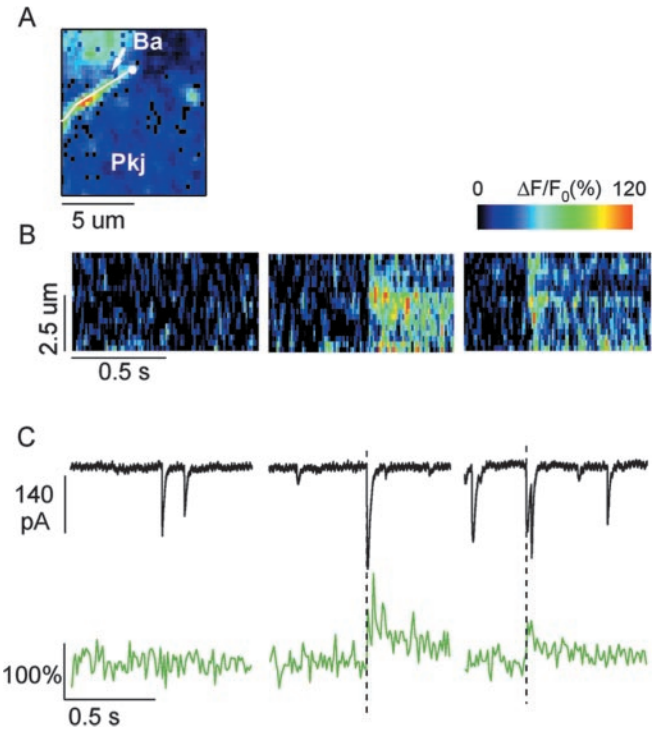

Figure 7. Simultaneous recording of Ca^{2+} transients in basket terminals and postsynaptic Purkinje cell IPSCs shows that synaptic transmission is maintained with the preloading technique. *A*, Average pseudocolor (in arbitrary units) fluorescence image from 100 scans obtained at rest from an 8×9 μm region containing a basket terminal (Ba) on a Purkinje cell soma (Pkj). *B*, Spatiotemporal profiles of the $[Ca^{2+}]$-dependent $\Delta F/F_0$ signals along the line drawn in *A*, showing two clear fluorescence transients in the second and third time series. *C*, Corresponding currents obtained from the Purkinje cell under voltage clamp at a holding potential of -68 mV (top traces) and $\Delta F/F_0$ transients analyzed in the basket terminal. Note that $\Delta F/F_0$ transients are correlated with the appearance of a postsynaptic IPSC.

preload). This factor is too small to totally account for the difference in dynamics that we measured. Another possible difference in the two configurations is a greater dialysis in whole-cell of one or more diffusible cytosolic components important for the regulation of Ca^{2+} dynamics.

Maintenance of synaptic transmission with presynaptic preloading

An important issue in this work was to investigate whether the axonal Ca^{2+} signals in preloaded cells could actually trigger neurotransmitter release. In three of the cases in which a terminal was identified on the soma of a Purkinje cell, it was possible to patch the postsynaptic cell. We could then record the fluorescence signals in the presumed terminal (Fig. 7*A*,*B*) in parallel with the spontaneous IPSCs in the postsynaptic cell. NBQX was added to the bath in these experiments. In all cases, the AP-evoked Ca^{2+} transients in the terminals were correlated to an IPSC (Fig. 7*C*). We estimated the probability that, given the frequency of spontaneous IPSCs, this correlation would just be attributable to chance. This probability was calculated as the probability of one IPSC to have its rise time within an imaging frame-time, raised to the power of the number of times the correlation was observed. The values in the three experiments were $p < 0.007$, $p \ll 0.0001$, $p < 0.01$ ($n = 5$, $n = 8$, and $n = 6$ events, respectively). This result indicates that the cell pairs were connected and that synaptic transmission caused by spontaneous AP firing in preloaded cells is preserved, even in the presence of the exogenous buffer fluo-4.

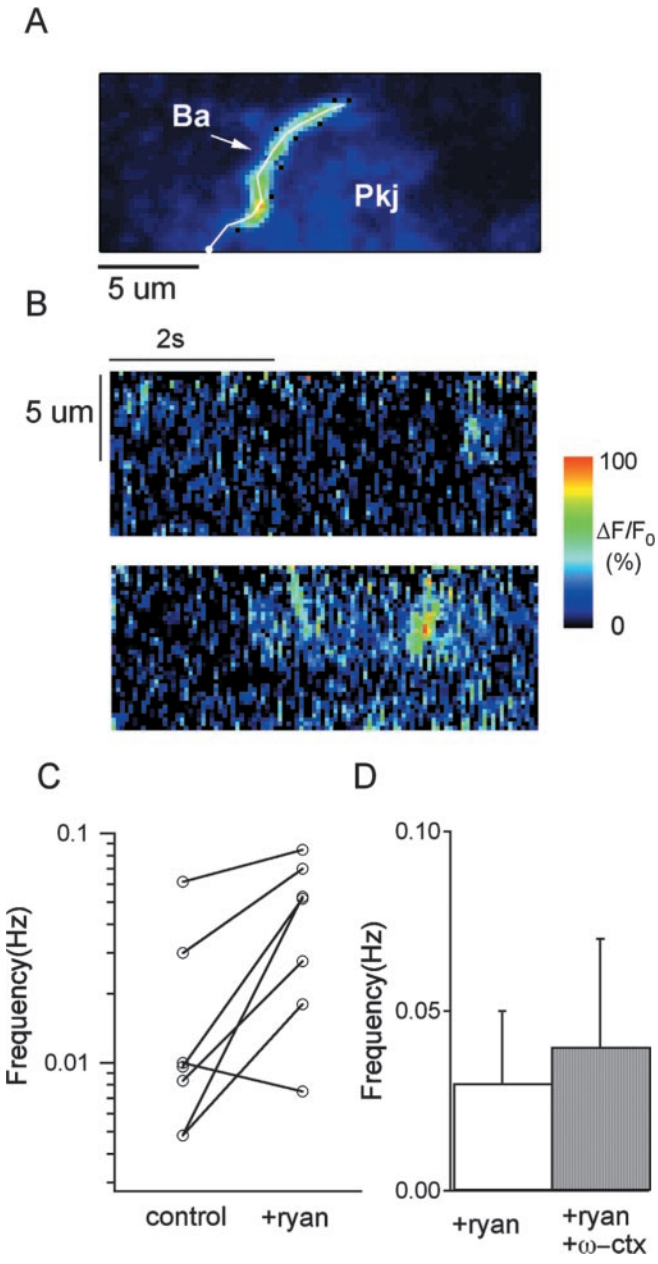

Figure 8. Ryanodine-sensitive SCaTs are present in preloaded basket terminals. *A*, Average pseudocolor (in arbitrary units) fluorescence image from 100 scans obtained at rest from a 23×9 μm region of a basket terminal (Ba) on a Purkinje cell soma (Pkj). *B*, Spatiotemporal profiles of the $\Delta F/F_0$ transients, calculated along the line drawn in *A* showing SCaTs recorded in 0.2 μM TTX, 6 mM Ca^{2+}, and 10 μM ryanodine. *C*, Average data (7 cells) on SCaT frequency before (control) and after addition of 10 μM ryanodine (+ryan) to the external solution, which contained 0.2 μM TTX and 6 mM Ca^{2+}. Each pair of connected points corresponds to individual cells. *D*, The average frequency of SCaTs at basket terminals is not influenced by bath application of the P/Q- and N-type VDCC blocker ω-conotoxin MVIIC as shown by the bars (avg $\pm$ sdev) from seven control cells during ryanodine application (+ryan) and four cells in which the toxin (at a concentration of 5 μM) was added together with 10 μM ryanodine (+ryan, +ω-ctx) ($p > 0.1$).

Ryanodine-sensitive SCaTs are observed in preloaded terminals

We next addressed the crucial question of whether ryanodine-sensitive SCaTs occurred in preloaded cells after firing activity was blocked by bath application of TTX. Once a connection was found, we used the same protocol as in whole-cell recordings to investigate whether SCaTs were present. During the initial period in BBS, it was often possible to measure Ca^{2+} fluctuations caused

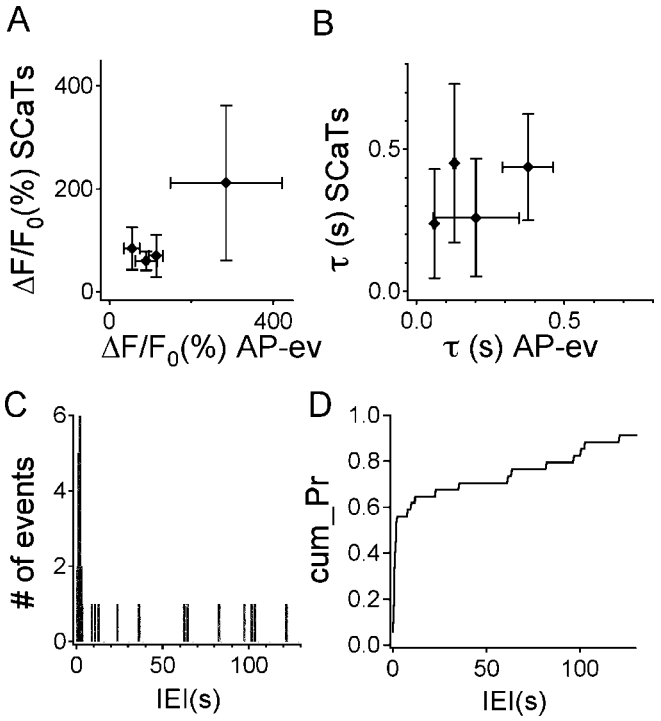

Figure 9. Comparison of AP-evoked signals and SCaT properties in preloaded basket cells. *A*, Average values for the peak $\Delta F/F_0$ of SCaTs (*y*-axis) and AP-evoked transients (*x*-axis) in four preloaded cells. *B*, Corresponding analysis for the time course of decay (τ) in the same experiments. Error bars represent SDs. *C*, *D*, Raw (*C*) and cumulative (*D*) histograms of IEIs between successive SCaTs, analyzed in four terminals of preloaded basket cells. Bin width for the raw histogram, 0.5 sec.

by spontaneous AP firing, as already discussed. These Ca^{2+} transients disappeared within 1 min from application of 0.2 μM TTX, 6 mM Ca^{2+}_o, after which all spontaneous fluorescence signals where taken as SCaTs. In 7 of 10 experiments, SCaTs could be observed in the terminals either in control or after addition of 10 μM ryanodine (Fig. 8*B*). Interestingly, in all experiments in which we detected spontaneous AP-mediated Ca^{2+} elevations in BBS, SCaTs could then be observed after application of ryanodine. In six of seven cells, SCaTs frequencies increased after addition of 10 μM ryanodine, whereas one experiment showed a small decrease (Fig. 8*C*). In three cells SCaTs were not observed during the control period, in which case the frequency was taken to be 1/(observation time in control). The average frequencies across cells thus obtained were 0.02 ± 0.02 and 0.04 ± 0.03 Hz in control and after addition of ryanodine ($n = 7$ cells). The average value of the ratio between frequencies in ryanodine versus control for each cell was 4.0 ± 3.5, indicating a significant increase in SCaTs frequency after ryanodine application (*t* test on the distribution of the log of the ratios: $p < 0.025$; $n = 7$ cells). These results show that SCaTs are present in basket terminals in a recording condition that is not influenced by prolonged dialysis. Moreover, their frequency and ryanodine dependence are comparable with those in whole-cell recordings.

Amplitude and time course of SCaTs

Two main drawbacks of the preloading technique are that the number of photons emitted from the sample is at the limit for signal detection and analysis and that the area of the recorded region is smaller. A more thorough characterization of amplitude and τ_{decay} of SCaTs was thus possible only in four of the seven cells in which the signals were sufficiently high and the site of origin of the SCaTs could be resolved within the imaged area. The average peak $\Delta F/F_0$ amplitude of SCaTs in the four preloaded cells was $106 \pm 70\%$, comparable with the amplitude of the signals caused by spontaneous AP firing in BBS ($136 \pm 100\%$) (Fig. 9*A*). Values for τ_{decay} of SCaTs in this configuration were slower than those of AP-evoked signals (Fig. 9*B*) (ratio of τ_{decay} for AP-evoked signals vs SCaTs: 0.54 ± 0.32; $p > 0.95$ of the ratio being <1; $n = 4$ cells). The values for SCaTs from different sites of origin in the same terminal were averaged together in this analysis and compared with the AP signals measured at the more responsive regions. Because of the small sampling of these fast transients and the desynchronization of the two-photon imaging with respect to the firing time of the cell, together with a strong compartmentalization of the fluorescence signals in preloaded cells, spontaneous firing did not always evoke a detectable Ca^{2+} elevation at the sites where SCaTs were observed.

SCaTs properties at the sites of origin

As in whole-cell recording, SCaTs in preloaded cells appeared clustered in time at each site. In these recordings we could distinguish even higher-frequency events than in whole-cell recordings, spaced in time by <400 msec (minimal detected interval: 200 msec). The IEI distribution and its cumulative probability, calculated for seven sites in four cells, shows that 50% of the events have IEIs of <1.5 sec (Fig. 9*C*,*D*). The faster decay times of the fluorescence signals in this recording configuration allowed us to distinguish multiple events that might have been difficult to separate in the whole-cell recordings, in which decay times were of the order of seconds. These results suggest that the increase in SCaTs frequency in ryanodine could be responsible for the increase in mIPSCs measured in Purkinje cells (Llano et al. 2000).

The preloading configuration allowed us to measure SCaTs at terminals in which vesicular release can occur. It would have been ideal to establish a direct correlation between the SCaTs and the mIPSC currents in the postsynaptic cell; however, this measurement did not give conclusive results in the few cases in which paired recordings were obtained. Because of the spatial restriction of SCaTs, recordings performed on small areas (6×9 μm; 10 msec per frame; 100 Hz) failed to capture the origin of the SCaTs and rendered it impossible to estimate their time of initiation. When larger areas were recorded (26×9 μm; 52 msec per frame; 20 Hz), the SCaTs spatial origin could be detected, but the lower temporal resolution of their rise time, together with their low frequency and the high frequency of mIPSCs in the Purkinje cell, did not allow us to make a correlation between the electrical and optical signals. In fact, the frequency of mIPSCs in the Purkinje cells is increased in these recording conditions, with half of the mIPSCs separated in time by <20 msec (Llano et al., 2000).

The role of voltage-dependent Ca^{2+} channels in the initiation of SCaTs

One possible trigger of CICR is calcium entry through voltage-dependent Ca^{2+} channels (VDCCs). We thus examined whether Ca^{2+} influx through VDCCs could be responsible for SCaTs generation. Although our experimental conditions in wcr (−78 mV holding potential in the voltage-clamp configuration and complete block of Na^+ channels by TTX) make it unlikely for VDCC to be active, their gating could take place in the preloading configuration, where there is no voltage control of the cell. We therefore investigated this possibility by direct block of VDCCs with bath application of 5 μM ω-conotoxin MVIIC (a saturating concentration for blocking P/Q and N channels), which has been reported to block the majority of the AP signals in these axons

(Forti et al., 2000). We first measured the effect of the toxin on the AP-evoked Ca^{2+} transients in our experimental conditions, in the wcr configuration. A series of four AP trains, as already described, were delivered every 1–2 min. After a control period of 9 min, the toxin was added to the bath while the stimulation protocol continued. The amplitude of the AP-evoked fluorescence responses promptly decreased, reaching a steady level within 4 min after drug application. The percentage decrease of the fluorescence response, measured between 4 and 6 min after drug application, varied from 51 to 78% (average ± SD = 60 ± 10%; $n = 4$ cells), in agreement with Forti et al. (2000).

To test directly for a possible role of VDCC on SCaTs initiation, we performed experiments on preloaded cells, in which VDCCs would be more likely to be activated. Experiments were conducted on five identified basket terminals of five different cells. Once a terminal was found, TTX and 6 mM Ca^{2+} were bath applied. After a short period, 5 μM ω-conotoxin MVIIC and 10 μM ryanodine were added. Data were analyzed in the time window between 4 and 12 min after drug application, when toxin block should have been maximal. SCaTs could be observed in four of five cells, at a frequency comparable with that obtained in the control preloading experiments (0.03 ± 0.02 Hz as compared with 0.04 ± 0.03 Hz; $p > 0.1$ of the two frequencies being the same) (Fig. 8*D*). Moreover, the average peak amplitude did not change (125 ± 109% in ω-conotoxin MVIIC, $n = 4$ cells, vs 106 ± 70% controls, $n = 4$ cells).

Discussion

SCaTs have been described briefly in this preparation previously (Llano et al., 2000). In the present work, we describe the properties of SCaTs in more detail. To investigate their functional relevance, we focused on identified basket terminals (rather than on the entire axon in our previous work), and we included results from preloaded cells (where synaptic transmission is preserved, as opposed to whole-cell recordings). Salient results are that (1) SCaTs are observed at basket terminals, with similar frequencies in preloaded cells and after prolonged whole-cell recordings; (2) SCaTs amplitudes are similar or larger than the Ca^{2+} signals elicited by action potentials, consistent with a potent role of SCaTs in the control of exocytosis; (3) VDCC blockers fail to affect SCaT frequency or amplitude; and (4) the sites of origin of SCaTs do not coincide with those of action potential evoked Ca^{2+} transients.

We showed that SCaTs are present in basket terminals of cells held at −78 mV in the whole-cell configuration and that their frequency is increased more than fourfold by application of low concentrations of ryanodine, as already observed in basket axons of the same preparation (Llano et al., 2000). On average, AP-evoked Ca^{2+} signals and SCaTs at the basket terminals have the same peak amplitude; however, at a given site, there is no correlation between these two quantities. The sites of origin of SCaTs had an average spacing of 6 μm, with a significantly higher probability of occurrence at axonal endings. Local maxima of Ca^{2+} response during AP firing, called "hot spots," were reported for cerebellar interneurons in axons coursing the molecular layer, at a relative distance of ~6 μm (Forti et al., 2000). Although we observed heterogeneities in the response to AP firing within these extended basket terminals, the sites of origin of SCaTs did not correlate with the maxima of AP fluorescence transients. This agrees with the notion that in the presence of TTX and at the imposed hyperpolarized potential, SCaTs are caused mostly by Ca^{2+} release from intracellular stores, whereas Ca^{2+} transients during AP firing arise mainly from VDCC activation, with RyRs contributing only ~23% (Llano et al., 2000). These results indicate that the spatial location and biophysical properties of the sources of calcium for the two types of signals are different.

Experiments conducted on preloaded cells allowed us to obviate two problems of the whole-cell configuration. First, we could verify that the two cells were connected by patching the Purkinje cell postsynaptic to an optically identified terminal. Second, we could measure SCaTs properties in terminals that are not affected by prolonged dialysis and show that their frequency dependence on ryanodine is similar to that observed in whole cell. In preloaded cells, SCaTs sometimes occurred in regions where AP evoked Ca^{2+} transients could not be detected reliably, and we were thus unable to compare their properties at the same site. Average peak amplitudes, when measured at the sites of maximal response for the two types of events, were similar in size. By comparing AP-evoked signals with SCaTs, we can infer that if ryanodine receptors are in close proximity to sites of vesicular release, calcium release from intracellular stores could significantly contribute to the generation of mIPSCs. In support of this notion, the increase of SCaTs frequency after application of ryanodine closely resembles the increase in frequency of mIPSC bursts in Purkinje cells by the same concentration of ryanodine (albeit at lower extracellular Ca^{2+} concentration) reported by Llano et al. (2000) and Bardo et al. (2003). Moreover, our finding that a selective blocker of P/Q- and N-type channels does not influence the frequency and amplitude of SCaTs is in agreement with the fact that Cd^{2+} and the specific P/Q-type channel blocker ω-Aga-IVA do not influence large mIPSCs in Purkinje cells (Llano et al. 2000).

The faster dynamics of the fluorescence transients recorded in the preloading configuration are explained in part by the lower concentration of the intracellular indicator, which we estimated to be half that in the whole-cell configuration, and by washout of intracellular components in whole cell. The endogenous calcium buffer parvalbumin (PV), which is present in these axons [in young mice (Caillard et al., 2000); our unpublished data on young rats] has a particularly slow binding constant for calcium ($k_{on} = 6\ \mu M^{-1}\ sec^{-1}$; $k_{off} = 0.9\ sec^{-1}$), which makes the properties of the calcium signals at these terminals different from those of axonal terminals in which PV is not present. Interestingly, PV concentration does not influence the fast rise and peak amplitude of calcium transients (Lee et al., 2000). Their amplitude (A) is determined by the indicator concentration and the physical properties of the sources following the equation: $A = [Q_{Ca}/(2FV)]/(1 + k'_B)$ [modified from Helmchen et al. (1997) in the approximation of no fast endogenous buffer], where Q_{Ca} is the total calcium entering the terminal, F is the Faraday constant, V is the volume accessible to Ca^{2+}, and k'_B is the incremental binding ratio of the indicator used. Because the average peak amplitude of the AP-evoked signals measured in preloaded cells was only twice that measured in the whole-cell configuration (111 vs 63%), the equation indicates a decrease of the Ca^{2+} binding ratio of the indicator to half its value, in agreement with our estimates of indicator concentration based on the resting fluorescence.

We found that SCaTs tend to appear in bursts. Similar bursts of ryanodine-sensitive calcium transients have been observed in heart muscle (Cheng et al., 1993) in the presence of low concentrations of ryanodine and in oligodendrocyte progenitor cells (Haak et al., 2001) after application of 3,7-Dimethyl-1-propargylaxanthine (a caffeine analog). The triggering mechanism for SCaTs in our system is not yet known, although direct and indirect evidence allow us to rule out some possible mecha-

nisms. Implication of ionotropic glutamate and $GABA_A$ receptors has been excluded (Llano et al., 2000). In the present work we exclude an involvement of VDCCs of the P/Q and N type by showing that bath application of a saturating concentration of ω-conotoxin MVIIC did not affect the frequency or amplitude of SCaTs. These channels are the main source of Ca^{2+} entry during AP firing in cerebellar interneurons (Forti et al., 2000), as confirmed by our present results with ω-conotoxin MVIIC.

In muscles, activation of RyRs is linked to L-type VDCCs either via Ca^{2+} influx (cardiac muscle) or by direct voltage-dependent mechanical coupling (skeletal muscle) (Pozzan et al., 1994; for review, see Niggli, 1999). The latter type of coupling has also been observed in neuronal cells (Chavis et al., 1996) and has been advanced as a plausible mechanism for the voltage-dependent "syntillas" in hypothalamic nerve terminals (De Crescenzo et al., 2004). In basket axons, no L-type channel contribution to AP-evoked Ca^{2+} rises has been measured (Forti et al., 2000). Moreover, SCaTs were observed during whole-cell recordings in TTX and at a hyperpolarized potential where VDCCs are either closed or inactivated (Hille, 2001). It is thus unlikely that L-type VDCCs are the triggering mechanism for SCaTs. A contribution of Ca^{2+} release from inositol trisphosphate receptor (IP_3R) activation to these signals or to their generation cannot be excluded. A possible induction mechanism for this pathway would be the activation of group I metabotropic glutamate receptors (mGluR), which could lead to IP_3 production (Berridge, 1998); however, mGluR1 and mGluR5 were not found in these axons at the adult stage (Baude et al., 1993; Negyessy et al., 1997), and a developmental study of mGluR1 distribution in Purkinje cells showed no evidence of these receptors at presynaptic structures from postnatal day 0 to adulthood (Lopez-Bendito et al., 2001). Intrinsic mechanisms, such as the state of Ca^{2+} filling of the stores and spontaneous fluctuations in the intracellular Ca^{2+} concentration, both of which will modulate IP_3Rs and RyRs (Pozzan et al., 1994; Berridge, 1998), could be at the basis of SCaT generation.

In oligodendrocyte progenitors, ryanodine-sensitive "sparks" and IP_3-mediated "puffs" coexist and are regulated by mitochondria activity, which presumably interferes with IP_3 production (Haak et al., 2002). In this system, Ca^{2+} release from intracellular stores is thought to be fundamental for neurite development, as suggested recently for various phenomena of neurite outgrowth (for review, see Rizzuto, 2001; Bouchard et al., 2003). Intracellular store release of Ca^{2+} has also been shown to contribute to the production of neurotrophic factor NT-3 in chick tectal axonal terminals (Wang et al., 2002). Moreover, a form of Ca^{2+}-dependent and TTX-independent vesicular release has recently been shown to be associated with membrane growth (Borgonovo et al., 2002). Interestingly, we found that axonal endings, which are still growing in 11–to 16-d-old animals (Pouzat and Hestrin, 1997), are preferential sites for SCaTs. The hypothesis of intracellular Ca^{2+} store signaling being a driving force for growth processes in basket terminals is relevant and would not conflict with their probable importance in the generation of mIPSCs. One of the hypothesized roles of miniature synaptic currents is that they are necessary for the stabilization and maintenance of synapses in the absence of neuronal activity (Turrigiano et al., 1998; Tyler and Pozzo-Miller, 2003).

References

Bardo S, Robertson B, Stephens GJ (2003) Presynaptic internal Ca^{2+} stores contribute to inhibitory neurotransmitter release onto mouse cerebellar Purkinje cells. Br J Pharmacol 137:529–537.

Baude A, Nusser Z, Roberts JD, Mulvihill E, McIlhinney RA, Somogy P (1993) The metabotropic glutamate receptor (mGluR1 alpha) is concentrated at perisynaptic membrane of neuronal subpopulations as detected by immunogold reaction. Neuron 11:771–787.

Berridge MJ (1998) Neuronal calcium signaling. Neuron 21:13–26.

Borgonovo B, Cocucci E, Racchetti G, Podini P, Bachi A, Meldolesi J (2002) Regulated exocytosis: a novel, widely expressed system. Nat Cell Biol 4:955–962.

Bouchard R, Pattarini R, Geiger JD (2003) Presence and functional significance of presynaptic ryanodine receptors. Prog Neurobiol 69:391–418.

Caillard O, Moreno H, Schwaller B, Llano I, Celio MR, Marty A (2000) Role of the calcium-binding protein parvalbumin in short-term synaptic plasticity. Proc Natl Acad Sci USA 97:13372–13377.

Carter AG, Vogt KE, Foster KA, Regehr WG (2002) Assessing the role of calcium-induced calcium release in short-term presynaptic plasticity at excitatory central synapses. J Neurosci 22:21–28.

Chavis P, Fagni L, Lansman JB, Bockaert J (1996) Functional coupling between ryanodine receptors and L-type calcium channels in neurons. Nature 382:719–722.

Cheng H, Lederer WJ, Cannel MB (1993) Calcium sparks: elementary events underlying excitation-contraction coupling in heart muscle. Science 262:740–745.

De Crescenzo V, ZhuGe R, Velázquez-Marrero C, Lifshitz LM, Custer E, Carmichael J, Lai FA, Tuft RA, Fogarty KE, Lemos JR, Walsh Jr JV (2004) Ca^{2+} syntillas, miniature Ca^{2+} release events in terminals of hypothalamic neurons, are increased in frequency by depolarization in the absence of Ca^{2+} influx. J Neurosci 24:1226–1235.

Diana M, Marty A (2003) Characterization of depolarization-induced suppression of inhibition using paired interneuron–Purkinje cell recordings. J Neurosci 23:5906–5918.

Emptage NJ, Reid CA, Fine A (2001) Calcium stores in hippocampal synaptic boutons mediate short-term plasticity, store-operated Ca^{2+} entry and spontaneous transmitter release. Neuron 29:197–208.

Forti L, Pouzat C, Llano I (2000) The spatial distribution of action potential-evoked Ca^{2+} signals in axons of developing rat cerebellar interneurones. J Physiol (Lond) 527:31–47.

Galante M, Marty A (2003) Presynaptic ryanodine-sensitive calcium stores contribute to evoked neurotransmitter release at the basket cell–Purkinje cell synapse. J Neurosci 23:11229–11234.

Haak LL, Song LS, Molinski TF, Pessah IN, Cheng H, Russel JT (2001) Sparks and puffs in oligodendrocyte progenitors: cross-talk between ryanodine receptors and inositol trisphosphate receptors. J Neurosci 21:3860–3870.

Haak LL, Grimaldi M, Smaili SS, Russell JT (2002) Mitochondria regulate Ca^{2+} wave initiation and inositol trisphosphate signal transduction in oligodendrocyte progenitors. J Neurochem 80:405–415.

Helmchen F, Borst JGG, Sakmann B (1997) Ca^{2+} dynamics associated with a single action potential in a CNS presynaptic terminal. Biophys J 72:1458–1471.

Hille B (2001) Ionic channels of excitable membranes. Sunderland, MA: Sinauer.

Koester HJ, Sakmann B (2000) Calcium dynamics associated with action potentials in single nerve terminals of pyramidal cells in layer 2/3 of the young rat neocortex. J Physiol (Lond) 529:625–646.

Krizaj D, Lai FA, Copenhagen DR (2003) Ryanodine stores and calcium regulation in the inner segment of salamander rods and cones. J Physiol (Lond) 547:761–774.

Lee SH, Schwaller B, Neher E (2000) Kinetics of Ca^{2+} binding to parvalbumin in bovine chromaffin cells: implications for $[Ca^{2+}]$ transients of neuronal dendrites. J Physiol (Lond) 525:419–432.

Lelli A, Perin P, Martini M, Ciubotaru CD, Prigioni I, Valli P, Rossi ML, Mammano F (2003) Presynaptic calcium stores modulate afferent release in vestibular hair cells. J Neurosci 23:6894–6903.

Lim R, Oleskevich S, Few AP, Leao RN, Walmsley B (2003) Glycinergic mIPSCs in mouse and rat brainstem auditory nuclei: modulation by ruthenium red and the role of calcium stores. J Physiol (Lond) 546:691–699.

Llano I, Marty A, Armstrong CM, Konnerth AM (1991) Synaptic- and agonist-induced excitatory currents of Purkinje cells in rat cerebellar slices. J Physiol (Lond) 434:182–213.

Llano I, González J, Caputo C, Lai AF, Blayney LM, Tan YP, Marty A (2000) Ryanodine-sensitive Ca^{2+} stores underlie large-amplitude miniature

IPSCs and spontaneous presynaptic Ca^{2+} transients at Purkinje cell synapses. Nat Neurosci 3:1256–1265.

Lopez-Bendito G, Shigemoto R, Lujan R, Juiz JM (2001) Developmental changes in the localization of the mGluR1α subtype of metabotropic glutamate receptors in Purkinje cells. Neuroscience 105:413–429.

Melamed-Book N, Helm PJ, Rahaminoff R (1993) Confocal microscopy reveals coordinated calcium fluctuations and oscillations in synaptic boutons. J Neurosci 13:632–649.

Narita K, Akita T, Osanai M, Shirasaki T, Kijima H, Kuba KA (1998) Ca^{2+}-induced Ca^{2+} release mechanism involved in asynchronous exocytosis at motor nerve terminals. J Gen Physiol 112:593–609.

Negyessy L, Vidnyanszky Z, Kuhn R, Knopfel T, Gorcs TJ, Hamori J (1997) Light and electron microscopic demonstration of mGluR5 metabotropic glutamate receptor immunoreactive neuronal elements in the rat cerebellar cortex. J Comp Neurol 385:641–650.

Neher E, Augustine GJ (1992) Calcium gradients and buffers in bovine chromaffin cells. J Physiol (Lond) 450:273–301.

Niggli E (1999) Localized intracellular calcium signaling in muscle: calcium sparks and calcium quarks. Annu Rev Physiol 61:311–335.

Palay SL, Chan-Palay V (1974) Cerebellar cortex: cytology and organization. Berlin: Springer.

Pouzat C, Hestrin S (1997) Developmental regulation of basket/stellate cell–Purkinje cell synapses in the cerebellum. J Neurosci 17:9104–9112.

Pozzan T, Rizzuto R, Volpe P, Meldolesi J (1994) Molecular and cellular physiology of intracellular calcium stores. Physiol Rev 74:595–636.

Rizzuto R (2001) Intracellular Ca^{2+} pools in neuronal signaling. Curr Opin Neurobiol 11:306–311.

Savic N, Sciancalepore M (1998) Intracellular calcium stores modulate miniature GABA-mediated synaptic currents in neonatal rat hippocampal neurons. Eur J Neurosci 10:3379–3386.

Simkus CRL, Stricker C (2002) The contribution of intracellular calcium stores to mEPSCs recorded in layer II neurones of rat barrel cortex. J Physiol (Lond) 545:521–535.

Tan YP, Llano I (1999) Modulation by K^+ channels of action potential-evoked intracellular Ca^{2+} concentration rises in rat cerebellar basket cell axons. J Physiol (Lond) 520:65–78.

Tan YP, Llano I, Hopt A, Würriehausen F, Neher E (1999) Fast scanning and efficient photodetection in a simple two-photon microscope. J Neurosci Methods 92:123–135.

Tyler WJ, Pozzo-Miller L (2003) Miniature synaptic transmission and BDNF modulate dendritic spine growth and form in rat CA1 neurons. J Physiol (Lond) 553:497–509.

Turrigiano GG, Leslie KR, Desai NS, Rutherford LC, Nelson SB (1998) Activity-dependent scaling of quantal amplitude in neocortical neurons. Nature 391:892–896.

Vincent P, Marty A (1996) Fluctuations of inhibitory postsynaptic currents in Purkinje cells from rat cerebellar slices. J Physiol (Lond) 494:183–199.

Wang XX, Butowt R, Vasko MR, Von Bartheld CS (2002) Mechanisms of the release of anterogradely transported neurotrophin-3 from axon terminals. J Neurosci 22:931–945.